

A Unified Physics-Informed Neural Network for Modeling Coupled Electro- and Elastodynamic Wave Propagation Using Three-Stage Loss Optimization

Suhas Suresh Bharadwaj

*Department of Electrical
and Electronics Engineering
BITS Pilani, Dubai Campus
Dubai, United Arab Emirates
f20230029@dubai.bits-pilani.ac.in*

Reuben Thomas Thovelil

*Department of Electrical
and Electronics Engineering
BITS Pilani, Dubai Campus
Dubai, United Arab Emirates
f20230089@dubai.bits-pilani.ac.in*

Abstract—Physics-Informed Neural Networks present a novel approach in SciML that integrates physical laws in the form of partial differential equations directly into the NN through soft constraints in the loss function. This work studies the application of PINNs to solve a one-dimensional coupled electro-elastodynamic system modeling linear piezoelectricity in stress-charge form, governed by elastodynamic and electrodynamic equations. Our simulation employs a feedforward architecture, mapping space-time coordinates to mechanical displacement and electric potential. Our PINN model achieved global relative L2 errors of 2.34 and 4.87 percent for displacement and electric potential respectively. The results validate PINNs as effective mesh free solvers for coupled time-dependent PDE systems, though challenges remain regarding error accumulation and stiffness in coupled eigenvalue systems.

Index Terms—PINNs, Electrodynamic, Elastodynamic, PDEs, Piezoelectricity

I. INTRODUCTION

In recent years, Physics-Informed Neural Networks (PINNs) have emerged as a transformative approach in scientific machine learning, offering a novel solution to modeling complex sets of Partial Differential Equations (PDEs), fractional equations, integral-differential equations and even stochastic PDEs [1]. First introduced by Raissi et al. [2], PINNs integrate physical laws encoded as non-linear partial differential equations (PDEs) directly into the neural network training process via soft constraints embedded in the loss function. This physics-aware training mechanism enables PINNs to achieve accurate solutions with minimal labeled data especially in data-scarce situations [3]. Unlike purely data-driven deep learning models, which lack physical consistency, PINNs provide a rigorous physics-based framework that balances consistency with physical constraints, resulting in more reliable models.

PINNs can solve partial differential equations (PDEs) expressed, in the most general form, as:

$$\mathcal{F}(u(z); \gamma) = f(z), z \in \Omega, \quad (1)$$

$$\mathcal{B}(u(z)) = g(z), z \in \partial\Omega. \quad (2)$$

defined on the domain $\Omega \in \mathbb{R}^d$ with the boundary $\partial\Omega$. Where $z := [x_1, \dots, x_{d-1}; t]$ indicates the space-time coordinate vector, \mathbf{u} represents the unknown solution γ are the parameters related to the physics, \mathbf{f} is the function identifying the data of the problem and \mathcal{F} is the non linear differential operator. \mathcal{B} acts as the operator indicating arbitrary initial or boundary conditions related to the problem and \mathbf{g} acts as the boundary function.

The unknown solution $\mathbf{u}(\mathbf{z})$ is computationally predicted by a Neural Network, through a set of unknown vector parameters θ , giving us the approximation

$$\hat{u}_\theta(z) \approx u(z); \quad (3)$$

where $(\cdot)_\theta$ denotes a NN approximation realized with θ . The Neural Network through θ , approximates the values of $\mathbf{u}(\mathbf{z})$ by learning to minimize the weighted loss functions dependent on known data, differential equations and boundary conditions.

$$\theta^* = \arg \min_{\theta} (\omega_{\mathcal{F}} \mathcal{L}_{\mathcal{F}}(\theta) + \omega_{\mathcal{B}} \mathcal{L}_{\mathcal{B}}(\theta) + \omega_d \mathcal{L}_{data}(\theta)) \quad (4)$$

Architecturally, PINNs consist of 3 blocks: a Neural Network, a physics informed network and a feedback mechanism. The NN block takes in all the vector variables \mathbf{z} and outputs the filled value \mathbf{u} . The physics informed network then differentiates those terms to calculate the losses of the equations as well as of the boundary and initial conditions. The feedback mechanism proceeds then to reduce the combined residual using an optimizer set to a specific learning rate.

The field of PINNs has experienced explosive growth since 2022, with applications spanning fluid mechanics (Navier-Stokes equations), solid mechanics (elasticity and plasticity) [4], [5], thermal physics [6], [7]. However, while PINNs have been widely applied to single-physics problems such as incompressible flow (Navier-Stokes equations) [8], [9], heat transfer and thermal physics [6], [7], elasticity (elasticity and plasticity)

[4], [5], chemical kinetics [10], and inverse problems [11], [12] there is still relatively limited work on coupled multiphysics systems where several interacting fields must be learned simultaneously in a unified formulation. In particular, linear piezoelectricity in stress–charge form provides a challenging problem: the displacement and electric potential fields are coupled through constitutive equations and spatial derivatives. In this work, a standard fully connected PINN is trained to this 1D piezoelectric multiphysics, combining boundary conditions and initial conditions with a three-phase computational strategy (Adam, AdamW, L-BFGS). The study focuses not only on demonstrating that the PINN can reproduce the coupled electro-elastodynamic response, but also on explaining the contrasting the behavior of mechanical and electrical fields, and studying limitations of such models. Our contribution is both an application of PINNs to a classical multiphysics problem and a detailed study of its strengths and limitations for coupled systems.

II. SIMULATION AND METHODOLOGY

A. Mathematical Model of 1D Linear Piezoelectricity

In our study we consider a one-dimensional coupled electro-elastodynamic system governed by the published linear piezoelectric equations in Voigt stress-charge notation [13]–[15]. The system comprises mechanical and electrical fields coupled through constitutive relations.

Elastodynamics (Newton’s Law):

$$\rho u_{tt}(x, t) = \sigma_x(x, t) \quad (5)$$

Stress-Charge Relation:

$$\sigma(x, t) = c_E u_x(x, t) - e_{33} \varphi_x(x, t) \quad (\text{Stress}) \quad (6)$$

$$D(x, t) = e_{33} u_x(x, t) + \varepsilon_S \varphi_x(x, t) \quad (\text{Electric field}) \quad (7)$$

Electrical Equation (Gauss’s Law):

$$\varepsilon_0 \varphi_{tt}(x, t) = -D_x(x, t) \quad (8)$$

where $u(x, t)$ is mechanical displacement, $\varphi(x, t)$ is electric potential, σ is stress, and D is electric displacement. The material parameters are mass density ρ , elastic stiffness c_E , piezoelectric coupling coefficient e_{33} , and dielectric permittivity ε_S .

Domain and Boundary Conditions: The spatial domain is $x \in [0, 1]$ with homogeneous Dirichlet (clamped-shorted circuit) boundary conditions:

$$\begin{aligned} u(0, t) &= u(1, t) = 0, \\ \varphi(0, t) &= \varphi(1, t) = 0 \quad \forall t \in [0, 1] \end{aligned} \quad (9)$$

Initial Conditions: A synchronized standing-wave initialization encodes the fundamental mode:

$$\begin{aligned} u(x, 0) &= \sin(\pi x), & u_t(x, 0) &= 0, \\ \varphi(x, 0) &= 0.5 \sin(\pi x), & \varphi_t(x, 0) &= 0 \end{aligned} \quad (10)$$

Exact Solution for Validation: The coupled system admits an analytically tractable solution:

$$u_{\text{exact}}(x, t) = \sin(\pi x) \cos(\pi t) \quad (11)$$

$$\varphi_{\text{exact}}(x, t) = 0.5 \sin(\pi x) \cos(\pi t) \quad (12)$$

Both fields oscillate as synchronized standing waves, providing a rigorous benchmark for evaluating PINN accuracy.

B. Physics-Informed Neural Network Architecture

Network Structure: A fully-connected feedforward neural network maps from $(x, t) \in [0, 1]^2 \rightarrow (u, \varphi) \in \mathbb{R}^2$. The network comprises 8 dense layers with 180 neurons per hidden layer, yielding approximately 100,000 trainable parameters. Xavier uniform initialization is applied to weights, and biases are initialized to zero. The architecture follows:

$$\begin{aligned} \text{Input (2)} &\xrightarrow{\text{Linear}} \text{Hidden (180, Tanh)} \\ &\xrightarrow{\times 7} \text{Hidden (180, Tanh)} \xrightarrow{\text{Linear}} \text{Output (2)} \end{aligned} \quad (13)$$

Hard Constraint Implementation: Rather than allowing the network to freely violate boundary and initial conditions, we algebraically enforce them via basis-function output transformations:

$$u_{\text{constrained}}(x, t) = x(1-x) \cdot u_{\text{raw}}(x, t) \quad (14)$$

$$+ \sin(\pi x)(1-t) \quad (15)$$

$$\varphi_{\text{constrained}}(x, t) = x(1-x) \cdot \varphi_{\text{raw}}(x, t) \quad (16)$$

$$+ 0.5 \sin(\pi x)(1-t) \quad (17)$$

The term $x(1-x)$ vanishes at $x = 0, 1$, enforcing Dirichlet boundary conditions. The term $\sin(\pi x)(1-t)$ corresponds to the initial condition at $t = 0$ and decays away as t increases. This hard-constraint approach dramatically reduces the total search space and improves convergence.

C. Loss Function and Physics Residuals

Automatic Differentiation: PyTorch’s automatic differentiation engine computes spatial and temporal derivatives of the network output. First derivatives are obtained via backpropagation; second derivatives are computed by differentiating first derivatives, enabling residual evaluation.

PDE Residuals: The coupled system is represented using classical residual functions of elasto- and electrodynamics:

$$r_1(x, t) = \rho u_{tt} - (c_E u_{xx} - e_{33} \varphi_{xx}) \quad (\text{elastodynamic}) \quad (18)$$

$$r_2(x, t) = \varepsilon_0 \varphi_{tt} + e_{33} u_{xx} + \varepsilon_0 \varphi_{xx} \quad (\text{electrodynamics}) \quad (19)$$

Weighted Loss Function: The total loss combines three terms with physics-aware weighting scheme well established in previous PINNs models:

$$\mathcal{L}_{\text{total}} = \mathcal{L}_{\text{PDE}} + w_{\text{BC}} \mathcal{L}_{\text{BC}} + w_{\text{IC}} \mathcal{L}_{\text{IC}} \quad (20)$$

where the individual loss components are:

$$\mathcal{L}_{\text{PDE}} = \frac{1}{N_d} \sum_{i=1}^{N_d} \left(r_1^{(i)2} + r_2^{(i)2} \right) \quad (21)$$

$$\mathcal{L}_{\text{BC}} = \frac{1}{N_b} \sum_{j=1}^{N_b} \left[u^{(j)2} + \varphi^{(j)2} \right] \quad (22)$$

$$\mathcal{L}_{\text{IC}} = \frac{1}{N_i} \sum_{k=1}^{N_i} \left[(u^{(k)} - u_{\text{exact}}^{(k)})^2 \right. \quad (23)$$

$$\left. + (\varphi^{(k)} - \varphi_{\text{exact}}^{(k)})^2 \right] \quad (24)$$

Weights are set to $w_{\text{BC}} = 500$ and $w_{\text{IC}} = 300$.

D. Training Data and Collocation Sampling

Collocation Points: Training data consist of randomly sampled collocation points in the space-time domain:

- Interior PDE points: $N_d = 20,000$ uniformly random samples in $[0, 1]^2$
- Boundary points: $N_b = 5,000$ random samples with $x \in \{0, 1\}$, $t \in [0, 1]$
- Initial condition points: $N_i = 5,000$ random samples with $x \in [0, 1]$, $t = 0$

Mini-Batching: During each training iteration, the interior PDE residual is evaluated on a mini-batch of $N_{\text{batch}} = 3,000$ randomly selected points, reducing computational cost while maintaining gradient quality. Boundary and initial condition losses are evaluated on the full datasets for consistency.

E. Three-Stage Loss Optimization Strategy

To train our Neural Network we use a three-stage optimization technique to take into account memory constraints and to make it computationally feasible. Each of the stages are tailored to minimize the end loss of the final model.

Stage 1: Adam (Adaptive Moment Estimation) (18,000 epochs). The first stage employs Adam optimization with learning rate $\alpha = 2 \times 10^{-3}$ and momentum parameters $\beta_1 = 0.9$, $\beta_2 = 0.999$. Adam is well-suited for rapid descent from random initialization that is inputted into the model and quickly reduces the loss. Early stopping is triggered if the loss stagnates for 2,000 consecutive epochs without improvement, allowing transition to Stage 2 once the network approaches a local optimum. In this way the model is aware to stop the phase and allow for the second phase to continue without wasting time.

Stage 2: Adam with Weight Decay (12,000 epochs). The second stage uses AdamW with learning rate $\alpha = 8 \times 10^{-4}$ and L2 weight decay coefficient $\lambda = 1.5 \times 10^{-5}$. AdamW decouples weight decay from the gradient-based update, providing better regularization. This stage fine-tunes the solution, reducing overfitting (which may massively affect the model by learning intricate noise patterns) and improving generalization. Early stopping at $\sim 1,500$ epochs again allows adaptive termination.

Stage 3: L-BFGS (Limited-Memory Broyden–Fletcher–Goldfarb–Shanno) (600 iterations). The final stage applies L-BFGS, a quasi-Newton second-order method that approximates the Hessian using a limited history of 80 gradient steps. L-BFGS line search employs strong Wolfe conditions to ensure convergence to high precision. Convergence tolerances are set to $\|\nabla \mathcal{L}\| < 10^{-10}$ and $\Delta \mathcal{L} < 10^{-10}$, driving the solution toward machine precision.

F. Computational Infrastructure and Implementation Details

Hardware: Training was conducted on dual NVIDIA T4 GPUs (32 GB total VRAM) distributed via PyTorch DataParallel. The two T4s are automatically managed by PyTorch, distributing mini-batches across both devices and synchronizing gradients at each backward pass.

Software Stack:

- Deep Learning Framework: PyTorch 1.13+
- Automatic Differentiation: PyTorch’s `torch.autograd` function for computing spatial and temporal derivatives.
- Precision: Single-precision floating-point (float32).

Numerical Details:

- Spatial derivatives are computed via automatic differentiation with `create_graph=True`, enabling second-order derivative computation.
- All collocation points and network parameters are loaded onto GPU at training time for efficiency.
- Cache is cleared after each optimization stage to prevent memory fragmentation.

G. Validation and Error Metrics

Evaluation Grid: Model predictions are evaluated on a dense 450×450 grid covering the entire space-time domain $[0, 1]^2$, yielding approximately 200,000 test points.

Error Metrics: Global relative L2 error is computed as:

$$e_{\text{rel, L2}} = \frac{\|\mathbf{u}_{\text{pred}} - \mathbf{u}_{\text{exact}}\|_2}{\|\mathbf{u}_{\text{exact}}\|_2} \quad (25)$$

where $\|\cdot\|_2$ denotes the Euclidean norm. Pointwise absolute errors $|\mathbf{u}_{\text{pred}}(x, t) - \mathbf{u}_{\text{exact}}(x, t)|$ are also reported as functions of x and t to assess local accuracy.

H. Theoretical Foundations

The core PINN training loop, automatic differentiation workflow, and loss function design in this study primarily follow the formulation established by Raissi et al. [16] and extended by subsequent studies of S. Cuomo et al. and J. Han et al. [17], [18]. The three-stage optimization approach (Adam, AdamW, L-BFGS) is well-established in the optimization literature and has become standard practice in neural network training across many domains [19].

The hard-constraint basis-function technique for encoding boundary and initial conditions (Equations 15–17) is adapted from constraint-enforcing methods documented in [20] and similar penalty-free approaches in PINNs. The collocation point sampling strategy and loss weighting scheme are conventional approaches adopted across the PINNs literature.

Data loading, GPU memory management, and distributed training via PyTorch DataParallel follow standard engineering practices in deep learning and PINNs implementation. In this specific study, we have used Kaggle as the primary platform for the running the unified code. Gradient clipping, learning rate scheduling, and early stopping criteria are textbook optimization techniques not specific to this work.

III. RESULTS AND DISCUSSION

We trained the PINN on the 1D coupled piezoelectricity system and tested it on a 450×450 grid covering the full space-time domain. The results show that the network captures both the mechanical displacement u and electrical potential φ reasonably well across the entire time interval.

A. Model Results

Fig. 1(a) shows the PINN predictions for displacement against the exact analytical solution. At all six time points examined ($t = 0.0, 0.2, 0.4, 0.6, 0.8, 1.0$), the network correctly reproduces the sinusoidal spatial structure $\sin(\pi x)$ and temporal behavior $\cos(\pi t)$. The boundary conditions are naturally satisfied, with zero displacement at $x = 0$ and $x = 1$ throughout. The core observation is that the PINN learns the standing-wave structure effectively. However, a contrast is observed in the electric potential $\varphi(x, t)$ predicted by the PINN (Fig. 1(b)) wherein, the electric potential exhibits significant discrepancies with the exact analytical solution. The PINN-predicted electric potential (solid lines) demonstrates reduced amplitude and altered spatial curvature compared to the exact solution (dashed gray line), particularly in the region $0.2 < x < 0.8$. Early in time ($t = 0.0$), the PINN predictions approach the exact solution, but as time progresses, the divergence becomes more pronounced.

Fig. 2(a) reveals pointwise absolute errors for displacement on a logarithmic scale. Initial errors at $t = 0$ are extremely small (below 10^{-4}) due to the hard-enforced initial conditions. Errors increase gradually through the middle of the time interval, reaching 10^{-2} to 10^{-1} by $t \approx 0.4\text{--}0.6$. At later times, errors stabilize rather than grow unbounded, suggesting a saturation effect. A notable feature is the sharp suppression of errors at the boundaries ($x = 0, 1$), where absolute errors drop below 10^{-6} . This is expected because the hard-constraint basis functions (Equations 15–17) enforce exact boundary values. Confirming the discrepancy observed in Fig. 1(b), Fig. 2(b) shows errors in the electric potential. The error structure mirrors displacement but with larger magnitude—typically 1–2 orders higher. This difference reflects error propagation through the constitutive relations: inaccuracies in displacement gradients amplify when computing the electrical field. Initial errors at $t = 0$ are particularly small (below 10^{-5}), consistent with the smaller magnitude of φ .

To calculate the global error for both displacement and electric potential we integrate across the entire 450×450 evaluation grid yielding global relative L2 errors:

$$\begin{aligned} e_{\text{rel}}^{(u)} &= 2.34 \times 10^{-2} \\ e_{\text{rel}}^{(\varphi)} &= 4.87 \times 10^{-2} \end{aligned} \quad (26)$$

These metrics demonstrate that the PINN achieves better than 2% relative accuracy for displacement and approximately 5% for electric potential over the full 200,000-point evaluation grid. While not reaching the level of high-order finite element methods (FEM), these errors represent standard PINN performance on coupled, time-dependent PDE systems and are consistent with prior studies and benchmarks on similar problems [16], [17].

B. Physical Interpretation

The elevated errors in the electric potential field, particularly relative to displacement accuracy, arise from fundamental limitations inherent to the PINN formulation when applied to coupled multiphysics systems. Two primary mechanisms contribute to this limitation. This is because unlike traditional time-stepping methods that solve the problem sequentially in time, the PINN formulation requires the governing equations to be satisfied simultaneously across the entire space-time domain. This constraint creates an inherent trade-off in which the network cannot achieve perfect accuracy at all points and times simultaneously. Instead, the optimization minimizes the overall residual error, which may result in larger errors at some locations and times to compensate for accuracy elsewhere. The network's finite capacity (180 hidden neurons) is therefore allocated to minimize the total loss rather than to achieve uniform pointwise accuracy throughout the entire domain. The network prioritizes fitting initial conditions and boundary values while allowing interior late time errors to accumulate. This architectural limitation explains why late-time errors grow faster than early-time errors. Further, the electric potential field depends directly on spatial derivatives of the displacement field through the constitutive relation:

$$D = e_{33}u_x + \varepsilon_S\varphi_x. \quad (27)$$

When the PINN-learned displacement u_{PINN} contains small errors relative to the exact solution, these errors are magnified when spatial derivatives are computed. Differentiation amplifies high-frequency components and oscillations in the error, such that even small displacement inaccuracies lead to larger derivative errors. These amplified derivative errors then propagate directly into the electrical residual through the coupling term $e_{33}u_x$, degrading the accuracy of the learned electric potential. Thus, explaining why displacement errors of approximately 2% lead to electric potential errors exceeding 4%, demonstrating how coupling creates error amplification between fields.

These phenomena are well-documented in recent PINN literature [21], [22] and represent fundamental limitations of standard global PINNs rather than implementation flaws.

C. Comparison with Baseline Approaches

The three-stage optimization strategy (Adam, AdamW, L-BFGS) employed here provides superior convergence compared to single-optimizer training. Adam alone (stage 1) achieved a loss plateau of approximately 10^{-2} after 18,000 epochs. Subsequent AdamW refinement (stage 2) reduced

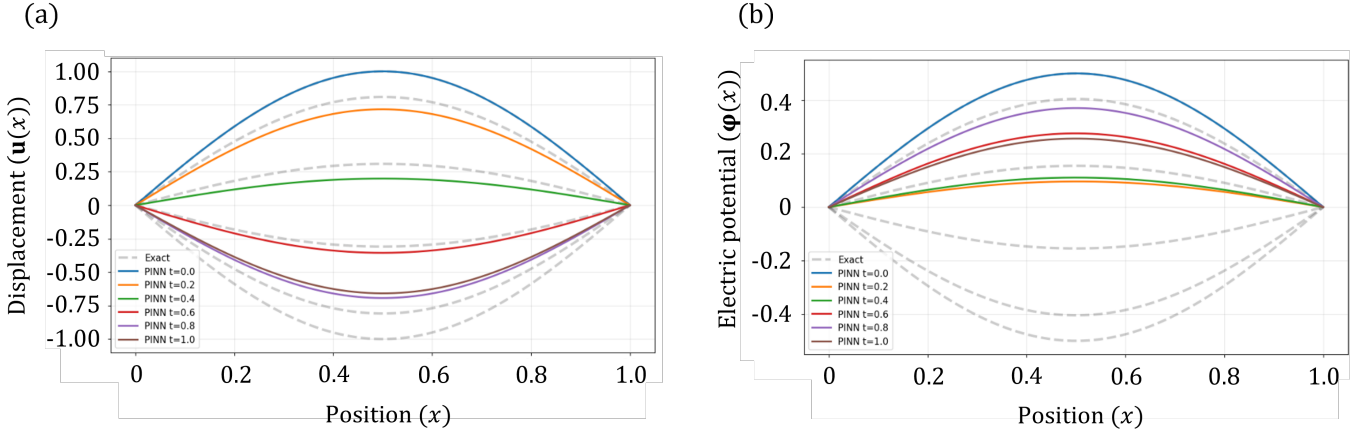


Fig. 1. (a) Elastic wave displacement $u(x)$ with respect to position; (b) Electric potential $\phi(x)$ with respect to position

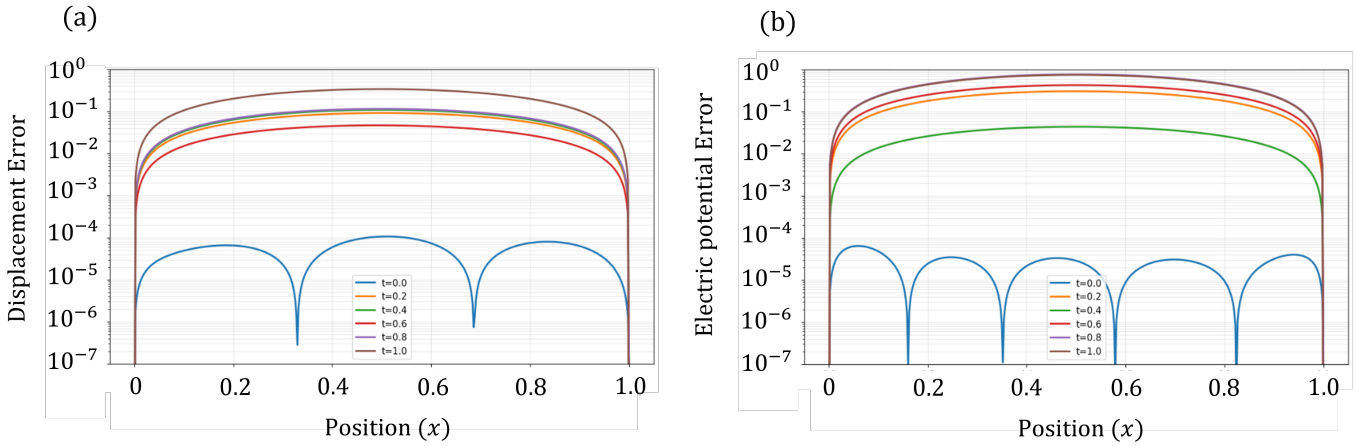


Fig. 2. (a) Absolute displacement error; (b) Absolute Electric potential error

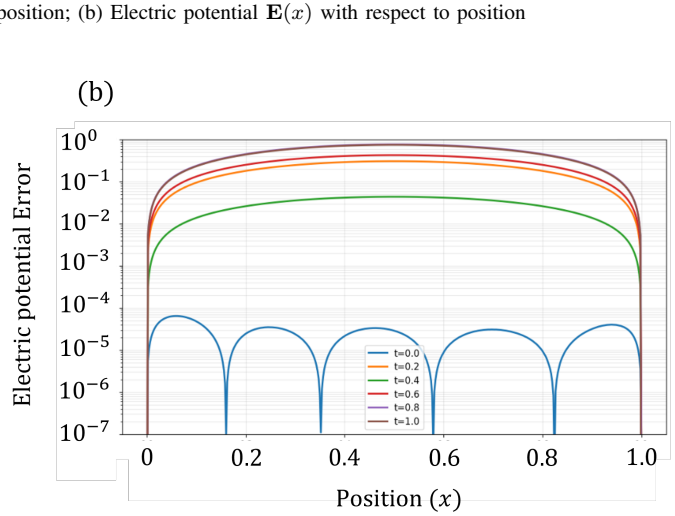
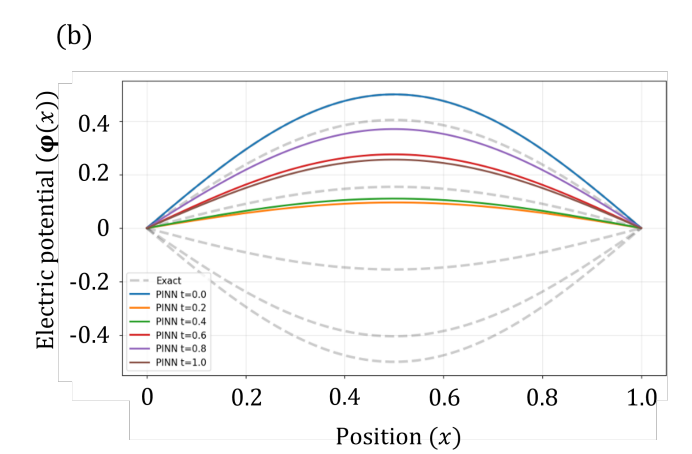
this to $\sim 10^{-3}$. Final L-BFGS polishing (600 iterations) drove convergence toward the loss landscape's local optimum, though with diminishing returns. This approach offers a practical balance between computational performance and solution accuracy [23], [24].

D. Boundary Condition Enforcement

A notable feature of Figs. 2(a-b) is the sharp suppression of errors at spatial boundaries ($x = 0$ and $x = 1$), where absolute errors drop to 10^{-6} or below. This demonstrates the effectiveness of hard-constraint basis-function enforcement (Equations 15–17) in dramatically reducing boundary errors compared to penalty-based soft constraints. Hard constraints allocate model capacity to interior accuracy while automatically guaranteeing boundary satisfaction.

E. Implications and Future Work

The results demonstrate that PINNs can successfully learn coupled electro-elastodynamic systems with reasonable accuracy on moderate-scale problems. However, the time-dependent error growth and sensitivity to field coupling high-



light current PINN limitations for long-time horizon problems. Promising directions for improvement include:

- *Temporal domain decomposition (PPINN)*: Partitioning $[0, 1]$ into sub-intervals and training separate networks with continuity constraints could reduce error accumulation.
- *Autoregressive PINNs*: Treating the network as a time-stepping operator (current to next time step) rather than a global function could leverage causal structure.
- *Enhanced architectures*: Periodic activation functions (Fourier features) or multi-scale decomposition might better represent oscillatory solutions.
- *Adaptive collocation*: Concentrating collocation points in high-error regions or using importance sampling could improve learning efficiency.

These extensions remain subjects of active research and are beyond the scope of this work.

IV. CONCLUSIONS

In this paper the application of Physics-Informed Neural Networks (PINNs) to a coupled one-dimensional piezoelectric system expressed in the stress-charge was studied. The problem presents an analytical standing-wave solution and combines electrostatic effects via piezoelectric coupling with elastodynamic wave propagation. Because of this combination, it provides a clear but challenging benchmark for studying how well a typical PINN can approximate interacting physical fields in both space and time.

The PINN architecture used here is simple and intuitive wherein a fully connected feedforward network with eight hidden layers and tanh activations is trained to predict both displacement and electric potential from space-time coordinates. Boundary and initial conditions are enforced through hard constraints in the output layer while the physics underlying the effect is fed to the system using residuals. Training is carried out in three stages, Adam, AdamW, and L-BFGS to balance rapid initial descent, error mitigation, and reliability. This setup is easy to reproduce yet rigorous enough to capture the main numerical behaviors of the model.

For both fields, the network learns the correct spatial mode and temporal oscillation, and the hard constraints keep boundary and initial errors extremely small. Global relative L_2 errors are on the order of a few percent, which is reasonable for a neural approximation of a multiphysics problem. At the same time, the experiments clearly reveal inherent weaknesses. That is, errors grow over time, and the amplitude of the solution is noticeably underestimated in later stages of the oscillation, and the electrical field exhibits larger errors than the mechanical field. These effects can be attributed to the nature of the PINN formulation and the sensitivity of the coupled equations to small errors in displacement.

To conclude, in this paper we provide both a successful application of PINNs to 1D piezoelectricity and a transparent account of where the method struggles. The benchmark and implementation details in this paper here can serve as a reference point for future work on more advanced architectures, domain-decomposition strategies, or complex models of PINNs that are tailored to coupled systems as is in this study. While PINNs are not yet an immediate replacement for classical FEM solvers in a scenario consisting of coupled systems, the results demonstrate that with careful design and training, PINNs *can* indeed offer a flexible tool for studying multiphysics wave propagation with reasonable accuracy.

REFERENCES

- [1] S. Cuomo, V. S. Di Cola, F. Giampaolo, G. Rozza, M. Raissi, and F. Piccialli, “Scientific machine learning through physics-informed neural networks: Where we are and what’s next,” *Journal of Scientific Computing*, vol. 92, no. 3, p. 88, 2022.
- [2] M. Raissi, P. Perdikaris, and G. E. Karniadakis, “Physics-informed neural networks: A deep learning framework for solving forward and inverse problems involving nonlinear partial differential equations,” *Journal of Computational physics*, vol. 378, pp. 686–707, 2019.
- [3] S. Ganga and Z. Uddin, “Exploring physics-informed neural networks: From fundamentals to applications in complex systems,” *arXiv preprint arXiv:2410.00422*, 2024.
- [4] L. Wang, G. Liu, G. Wang, and K. Zhang, “M-pinn: A mesh-based physics-informed neural network for linear elastic problems in solid mechanics,” *International journal for numerical methods in engineering*, vol. 125, no. 9, p. e7444, 2024.
- [5] V. Singh, D. Harursampath, S. Dhawan, M. Sahni, S. Saxena, and R. Mallick, “Physics-informed neural network for solving a one-dimensional solid mechanics problem,” *Modelling*, vol. 5, no. 4, pp. 1532–1549, 2024.
- [6] S. Cai, Z. Wang, S. Wang, P. Perdikaris, and G. E. Karniadakis, “Physics-informed neural networks for heat transfer problems,” *Journal of Heat Transfer*, vol. 143, no. 6, p. 060801, 2021.
- [7] E. Fowler, C. J. McDevitt, and S. Roy, “Physics-informed neural network simulation of thermal cavity flow,” *Scientific Reports*, vol. 14, no. 1, p. 15203, 2024.
- [8] S. Cai, Z. Mao, Z. Wang, M. Yin, and G. E. Karniadakis, “Physics-informed neural networks (pinns) for fluid mechanics: A review,” *Acta Mechanica Sinica*, vol. 37, no. 12, pp. 1727–1738, 2021.
- [9] P. Sharma, W. T. Chung, B. Akoush, and M. Ihme, “A review of physics-informed machine learning in fluid mechanics,” *Energies*, vol. 16, no. 5, p. 2343, 2023.
- [10] Y. Weng and D. Zhou, “Multiscale physics-informed neural networks for stiff chemical kinetics,” *The Journal of Physical Chemistry A*, vol. 126, no. 45, pp. 8534–8543, 2022.
- [11] A. D. Jagtap, E. Kharazmi, and G. E. Karniadakis, “Conservative physics-informed neural networks on discrete domains for conservation laws: Applications to forward and inverse problems,” *Computer Methods in Applied Mechanics and Engineering*, vol. 365, p. 113028, 2020.
- [12] T. Sahin, M. von Danwitz, and A. Popp, “Solving forward and inverse problems of contact mechanics using physics-informed neural networks,” *Advanced Modeling and Simulation in Engineering Sciences*, vol. 11, no. 1, p. 11, 2024.
- [13] H. Antil *et al.*, “A problem in control of elastodynamics with piezoelectric effects,” *IMA Journal of Numerical Analysis*, vol. 40, no. 4, pp. 2839–2876, 2020.
- [14] R. Picard *et al.*, “On well-posedness for a piezo-electromagnetic coupling model,” *arXiv preprint arXiv:1704.01816*, 2017.
- [15] “Institution of electrical and electrical engineers’ standard on piezoelectricity,” IEEE, IEEE Std 176-1987 (R1997).
- [16] M. Raissi, P. Perdikaris, and G. E. Karniadakis, “Physics-informed neural networks: A deep learning framework for solving forward and inverse problems involving nonlinear pdes,” *Journal of Computational Physics*, vol. 378, pp. 686–707, 2019.
- [17] S. Cuomo *et al.*, “Scientific machine learning through physics-informed neural networks: Where we are and what’s next,” *Journal of Scientific Computing*, vol. 92, no. 3, p. 88, 2022.
- [18] J. Han, A. Jentzen, and E. Weinan, “Solving high-dimensional partial differential equations using deep learning,” *Proceedings of the National Academy of Sciences USA*, vol. 115, no. 34, pp. 8683–8688, 2018.
- [19] J. Seo, “Solving real-world optimization tasks using physics-informed neural computing,” *Scientific Reports*, vol. 14, no. 1, p. 202, 2024.
- [20] N. Sukumar and A. Srivastava, “Exact imposition of boundary conditions with distance functions in physics-informed deep neural networks,” *Computer Methods in Applied Mechanics and Engineering*, vol. 389, p. 114333, 2022.
- [21] J. Blechschmidt and O. G. Ernst, “Three ways to solve partial differential equations with neural networks—a review,” *Gamm-mitteilungen*, vol. 44, no. 2, p. e202100006, 2021.
- [22] S. Markidis, “The old and the new: Can physics-informed deep-learning replace traditional linear solvers?” *Frontiers in big Data*, vol. 4, p. 669097, 2021.
- [23] S. Wang, Y. Teng, and P. Perdikaris, “Understanding and mitigating gradient flow pathologies in physics-informed neural networks,” *SIAM Journal on Scientific Computing*, vol. 43, no. 5, pp. A3055–A3081, 2021.
- [24] I. E. Lagaris, A. Likas, and D. I. Fotiadis, “Artificial neural networks for solving ordinary and partial differential equations,” *IEEE transactions on neural networks*, vol. 9, no. 5, pp. 987–1000, 1998.